www.czasopisma.pan.pl PAN POLSKA AKADEMIA NAUK www.journals.pan.pl

Arch. Metall. Mater. **68** (2023), 4, 1291-1299

DOI: https://doi.org/10.24425/amm.2023.146194

F. WANG[1], M. YANG[2*]

EFFECT OF COLLOID WATER THICKNESS ON MICROSTRUCTURES AND MECHANICAL PROPERTIES OF TITANIUM/STEEL INTERFACES PREPARED BY EXPLOSIVE WELDING

Using colloid water as a covering for explosives can improve the energy efficiency for explosive welding, while its effects on bonding properties remain unclear. Here, by employing titanium/steel as a model system, the effect of covering thickness on microstructures and mechanical properties of the bonding interface was systematically investigated. It was found that all the welds displayed wavy interfaces, and the wave size increased with increasing covering thickness. Vortices characterized by solidified melt zones surrounded by strongly deformed parent materials, were only formed for the welds performed with a covering. Moreover, with increasing covering thickness, both the tensile strength and the elongation of the titanium/steel plate decreased, and the failure mode changed from ductile to cleavage fracture, gradually. In the tensile-shear tests, all the fractures took place in titanium matrix without separation at interface, indicating that the titanium/steel interfaces had an excellent bonding strength. The micro-hardness decreased with increasing distance from the interface, and this trend was more remarkable for a thicker covering. The micro-hardness inside the solidified melt zones was far higher than that observed in strain-hardened layers of the parent metal, due to formation of hard intermetallic compounds.

Keywords: Explosive welding; Covering; Microstructure; Mechanical properties

1. Introduction

Ti alloys are characterized by good light weights, excellent corrosion resistances, and outstanding mechanical properties, which are used as construction materials in the fields such as power generation, aerospace, and chemical industries [1,2]. Nevertheless, wider use of these materials has been limited by their high costs. Steel is one of the common materials in our daily life, which exhibits low costs and excellent mechanical properties, such as high strength, hardness, and wear resistance. Thus, the fabrication of a layered Ti alloy and steel composite is considered attractive because it combines the respective merits of the two metallic components [3]. However, welding of Ti alloys and steel is challengeable due to potential technical problems such as existence of brittle intermetallic compounds and metallurgical incompatibility [4,5].

Several methods, such as friction welding [1,6,7], laser welding [8,9], diffusion bonding [10,11], roll bonding [3,12], and explosive welding [13-22], have been investigated for joining Ti alloys and steel. Among some techniques, they are difficult to obtain a complete metallurgical bond due to the absence of solid solubility between Fe and Ti, and formation of brittle intermetallic phases such as FeTi and Fe_2Ti [1,5]. Explosive welding is a widely used solid state joining technology, which produces a metallurgical bond between two layers of metal, aided by high-speed oblique collision induced by explosion [23]. During the oblique collision process, a high-speed jet is first formed between the metal plates, which can sweep away the oxide film that is detrimental to formation of the metallurgical bond, and then the virginally clean surfaces are bonded together under very high pressure [24,25]. The time gap of these processes is very short (~10^{-6} s), therefore heat transfer cannot be observed between the metallic plates [26,27]. Thus, explosive welding is characterized by high bonding strength and capability to keep the physical and chemical properties of the wrought parent components unchanged [23,28]. Therefore, explosive welding is the optimum selection for producing the titanium/steel joints.

The quality of bond strongly depends on the process parameters. There are three main dynamic parameters of explosive

[1] ANHUI UNIVERSITY OF SCIENCE AND TECHNOLOGY STATE KEY LABORATORY OF MINING RESPONSE AND DISASTER PREVENTION AND CONTROL IN DEEP COAL MINES, HUAINAN, ANHUI PROVINCE, CHINA
[2] NANJING UNIVERSITY OF SCIENCE AND TECHNOLOGY, NATIONAL KEY LABORATORY OF TRANSIENT PHYSICS, NANJING, 210094, CHINA

* Corresponding author: ym1991@mail.ustc.edu.cn

welding, i.e., collision angle β, collision point velocity V_c and impact velocity V_p, which are determined by initial parameters such as detonation velocity, stand-off distance, and explosive thickness. Mousavi et al. [19] investigated the effects of explosive loading on the microstructures of the interface morphology of cp-titanium/AISI 304 stainless steel using experimental methods, and presented an analytical calculation for determination of welding window. Durgutlu et al. [29] investigated the effect of the stand-off distance on interface characteristics of explosively welded copper/steel composite, and found that increasing the stand-off distance transformed the bonding interface from smooth to wavy shape. Manikandan et al. [14] employed a thin stainless steel plate as an interlayer in explosively welding of titanium and stainless steel plate to reduce the kinetic energy loss and the formation of intermetallic layer at the interface. Mendes et al. [28] studied the influence of explosive characteristics on the weld interfaces of stainless steel AISI 304L to low alloy steel 51CrV4 in a cylindrical configuration. The results showed that the type of explosive and sensitizers could affect the main welding parameters.

In our previous work, it was found that using colloid water as a covering for explosives could improve the energy utilization ratio and reduce the noise and dust of explosive welding. However, the previous studies focused on secondary hazards too much, while the influence of the colloid water layer on the bonding properties is still unclear. Thus, to obtain a better understanding of the effect of the covering on the welding quality and give a guidance of practical application, the experiments were carried out with various covering thicknesses and constant other parameters. The microstructure evolution in the interface was conducted by Light Microscopy and Scanning Electron Microscope (SEM) equipped with Energy-dispersive X-ray spectrometry (EDS). Furthermore, the mechanical properties of the weld plate were also evaluated by systematically mechanical tests.

2. Experiment

2.1. Experimental materials

As shown in Fig. 1, honeycomb structure explosives were employed as the explosive materials in this work, which were consisted of aluminium honeycomb filled with emulsion explosives in regular hexagon cells. Honeycomb structure is one of the most stable structures in nature, which can help to improve the compressive strength of the soft emulsion explosives, and guarantee the uniformity of explosives under the gravity of a covering. The emulsion explosives are composed of 75% emulsion matrix and 25% hollow glass microballoons, and the components of the emulsion matrix are presented in TABLE 1. The thickness of aluminium foil for making aluminum honeycomb is 60 μm and the side length of the regular hexagon cell is 6 mm. The height of aluminum honeycomb (the vertical distance between the upper and lower planes of the honeycomb plate) is 8 mm, which is equal to that of emulsion explosives. The densities and detonation velocities of the honeycomb structure explosives are about 0.85 g/cm^3 and 2900 m/s respectively.

As shown in Fig. 2, colloidal water was employed as the covering materials for explosives, which was composed of 1% Super Absorbent Polymer (SAP) and 99% water, and the density was 0.97 g/cm^3. SAP is a crosslinked acrylic acid/sodium acrylate copolymer, which can absorb water hundreds of times more than its own weight and has excellent water retention performance. The colloidal water is granular and behaves as a solid, so it is easy to precisely control the covering thickness, and there is no potential risk such as flying stone during the explosion process.

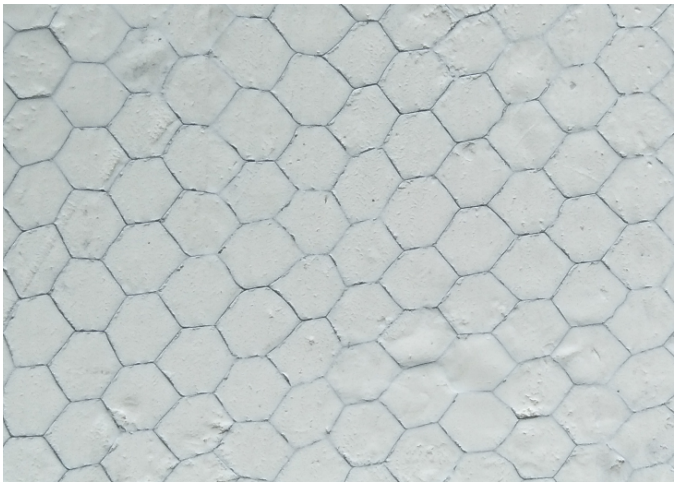

Fig. 1. Honeycomb structure explosives

TABLE 1

Composition of the emulsion matrix

Composition	NH_4NO_3	$NaNO_3$	H_2O	$C_{18}H_{38}$	$C_{24}H_{44}O_6$	$C_{12}H_{26}$
Mass fraction	75%	10%	8%	4%	2%	1%

Fig. 2. Colloidal water used in the tests

The materials of flyer plate and base plate were TA2 titanium and Q235 steel (grades: B), respectively. The dimensions of titanium and steel plates used were 150 mm × 100 mm × 2 mm and 150 mm × 100 mm × 20 mm, respectively. The surfaces of the base and flyer plates were ground with emery papers up to No. 400, after which they were cleaned by absolute ethyl alcohol. Their chemical compositions are given in TABLE 2 and TABLE 3, and the physical properties are shown in TABLE 4.

TABLE 2

Chemical composition of TA2 (wt%)

Element	Fe	Si	C	N	H	O	Ti
Content	≤0.30	≤0.15	≤0.10	≤0.05	≤0.02	≤0.2	Bal.

TABLE 3

Chemical composition of Q235 steel (wt%)

Element	C	Si	Mn	S	P	Fe
Content	≤0.14-0.22	≤0.30	≤0.30-0.65	≤0.05	≤0.05	Bal.

TABLE 4

The physical properties of Q235 and TA2

Material	ρ/(kg·m^{-3})	H_v/MPa	c/(m·s^{-1})	σ_b/MPa	T_m/°C
Q235B	7850	1500	6000	405	1493
TA2	4500	1800	6100	280	1660

Note: ρ is the density, H_v is the Vickers hardness, c is the sonic speed, σ_b is the tensile strength, and T_m is the melting temperature.

2.2. Experimental methods

Fig. 3 shows a schematic diagram of explosive welding in this work. The parallel set-up geometry located on a steel anvil was employed in all experiments, and all explosion were carried out in a cylindrical explosion vessel with 2.5 m in diameter and 5 m in length. Unlike the ordinary explosive welding setup, colloidal water was employed to cover the upper surfaces of the explosives. The thickness of the colloidal water is an important factor that affects the experimental results. Thus, five groups of tests were carried out with different covering thicknesses, and the initial parameters of the explosive welding are listed in TABLE 5, in which the collision point velocities were determined experimentally, and the impact velocities were calculated according to the previous study [30].

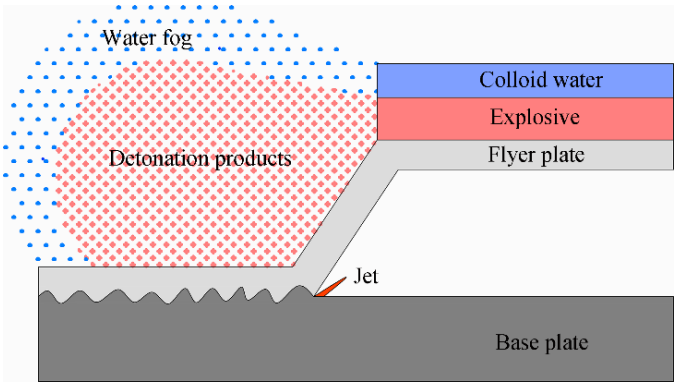

Fig. 3. Diagram of the explosive welding process

TABLE 5

Selected parameters for explosive cladding

Test No.	T_c/(mm)	S/(mm)	T_e/(mm)	V_c/(m/s)	V_p/(m/s)
1	0	8	8	2518	445
2	15	8	8	2636	582
3	30	8	8	2699	629
4	60	8	8	2717	657
5	100	8	8	2739	674

Note: T_c is the thickness of colloidal water, S is the gap between the flyer and *base* plates, T_e is the thickness of explosive, V_c is the collision point velocity, V_p is the impact velocity.

To reveal the interface morphologies, specimens were cut parallel to the detonation direction, and the cross-sections of the specimens were ground with emery papers up to No. 5000 and polished to 0.5 μm by diamond paste. Then, the specimens were etched by etchant consisting of hydrofluoric acid and nitric acid. A scanning electron microscope (GeminiSEM 500) and a light microscope (Leica DM4M) were employed for microstructure observation of the bonding interfaces. Energy-dispersive X-ray spectrometry (EDS) analysis was also done to characterize the distribution of the alloy elements across the bonding interfaces.

In order to investigate the mechanical properties of the welded plates, microhardness, tensile, and tensile-shear tests were carried out. Microhardness tests were conducted on a microhardness machine (HVS-1000M) using a 100 g load for 10 s. The tensile and tensile shear tests were carried out with a tensile strain rate of 1×10^{-4}/s according to GB/T6396-2008 [31], and the dimensions of the specimens are shown in Fig. 4. Three samples were tested for tensile and tensile shear tests, and the average values are reported. Fractography studies on broken specimens from tensile tests were carried out using a scanning electron microscope.

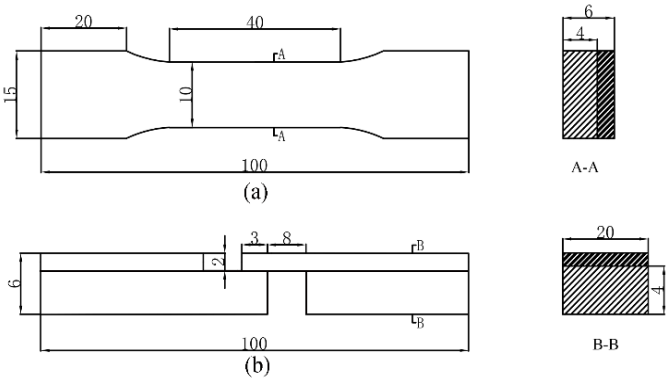

Fig. 4. Dimensions of the tensile specimen (a) and tensile-shear specimen (b)

3. Results and discussion

3.1. Microscopic observations

Fig. 5 shows the light microscope images of TA2/Q235 bimetallic sheets. Fig. 5a and b are the microstructures of Q235 steel and TA2 titanium away from the bonding interface (Test No. 3, T_c = 30 mm), which indicated that the Q235 steel is mainly composed of equiaxed pearlite with ferrite, and the TA2 titanium is characterized by fully equiaxed α-Ti grains. Fig. 5c-g are microstructures of TA2/Q235 bonding interfaces for different covering thicknesses, which show that all the welds display wavy interfaces. For titanium/steel explosively bonding interface, both straight and wavy interfaces could be found in previous studies [18-21]. Because the wavy pattern can provide mechanical locking between the flyer and base plates, the wavy interfaces usually have higher bonding strength [32,33]. The wave formation can be attributed to the results of hydrodynamic behavior of interfacial materials and variations in the velocity distribution at collision point [14,34]. The hydrodynamic behavior is due to the pressure in collision region being many times higher than the dynamic yield strength of the metals, and the variations in the velocity distribution are related to oscillatory nature of the propagation of detonation wave. Fig. 6 shows the effect of covering thickness on wavelength and amplitude of weld, where the wavelength and amplitude are the average values determined by five waves, which indicates that the wavelength and amplitude both increased with the increase of covering thickness. Deribas et al. stated that the wavelength increased with the increase in any one of the parameters: loading ratio, collision angle, flyer plate velocity, stand-off distance, and thickness of base plate [35]. Thus, the increase in wavelength and amplitude in this work can be related to the impact velocities increasing with the increase of covering thickness, as shown in TABLE 5. This result was similar to the previous studies [19,27,29,34].

It can be also seen from Fig. 5c-g that vortices (dark regions under the curl of the waves) were formed for the welds performed with a covering, while they were not found in welds performed with no covering. The reason for this was that impact velocity of the flyer plate performed with a covering is higher, which resulted in stronger plastic flow, and similar results could be found in previous studies [19,36]. These vortices are characterized by large volumes of solidified melt surrounded by strongly deformed bulk materials, as shown in Fig. 5h and i. The melt zones are of fundamental importance for the clad properties due to the unique phase structure and formation of defects such as

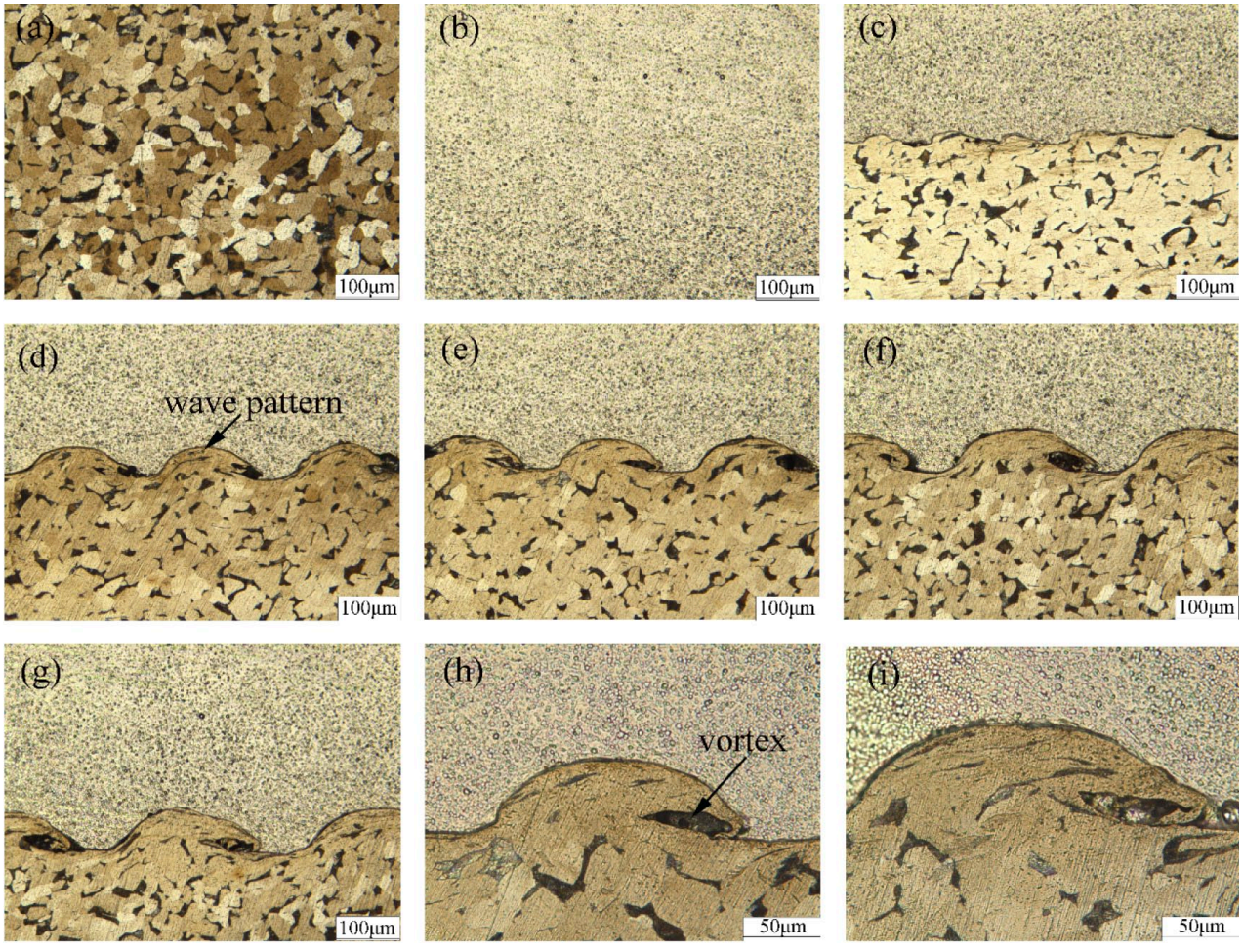

Fig. 5. Light microscope images of TA2/Q235 bimetallic sheet, (a) Q235 steel away from the interface, (b) TA2 titanium away from the interface, (c-g) TA2/Q235 bonding interface for different covering thicknesses: (c) T = 0 mm, (d) T = 15 mm, (e) T = 30 mm, (f) T = 60 mm, (g) T = 100 mm, (h) typical vortex from covering thickness of 60 mm, (i) typical vortex from covering thickness of 100 mm

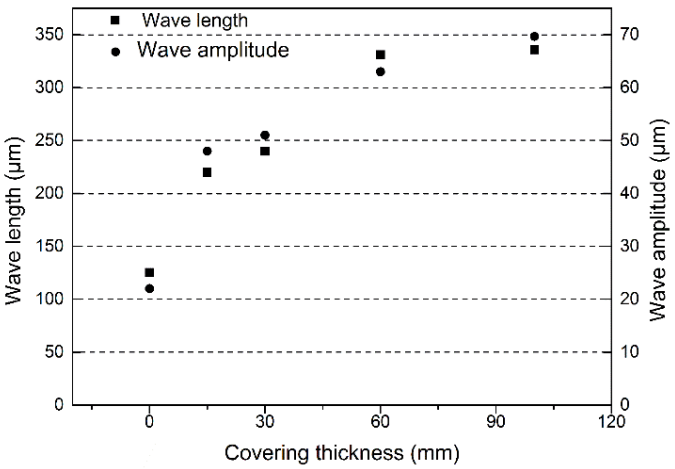

Fig. 6. Effect of the thickness of the colloidal water on wavelength and amplitude of the bonding interface

micropores and cracks [41]. Additionally, it should be noted that the solidified melt zones can also appear as a thin layer along the whole interface. In the work of Paul et al. [41], it was found that the continuous melt layers are only 0.5 ~ 1.0 μm in thickness, so they are not visible by light microscope used in this work. However, the extremely thin layer of solidified melt was typically observed in previous works, where TEM techniques were used to study the interfacial properties of Cu/Al [37], Ta/stainless steel [41], and Zr700/carbon steel clads [42], et al. The formation of the solidified melt zone could be due to rapid temperature boost at the bonding interface, induced by intense plastic flow, shear, and friction between the two metals. According to the numerical simulations performed by Bataev et al. [43] and Chu et al. [21], the temperature near the collision point was estimated to be ~2000°C, which significantly exceeded the melting point of joined metals. Because there is no time for heat transmission, the melted zones were surrounded by relatively cold materials and subjected to an extremely high cooling rate. Obviously, the cooling rate varied with temperature and time, and the highest cooling rates was estimated to be of the order of 10^7-10^9 K/s [37,41,43]. The high temperature and subsequently rapid cooling give the opportunity to formation of distinct structures such as intermetallics, ultra-fine grains and metallic glasses, and more detailed discussions on this topic can be found in previous studies [42-44].

In order to further study the properties of the localized melting zones, EDS was carried out to characterize the distribution of the alloy elements across the bonding interface. Fig. 7a, b and c show the EDS mapping near a vortex, which indicates that the chemical composition of the vortex is different from those of TA2 titanium and Q235 steel. This result was in agreement with the previous studies [15] about element diffusion on the Ti/Fe interface after explosive welding. Fig. 7d shows the results of element spot scans near the bonding interface. It was found that the vortex contained both the base and flyer plate materials, which indicated that the participant metals were intensely mixed during the collision process. According to the previous studies [38], the intermetallic compounds such as TiFe and Ti_2Fe were usually formed in the vortex, which are characterized by brittleness. In this condition, microcracks are usually induced due to the rapid solidification and further cooling of the dissimilar partners with different thermal expansion coefficients [13]. It can also be seen from Fig. 7d that the content of Fe in the vortex is significantly higher than that of Ti. This is due to the deflection of the jet away from the plate of lower density, impingement occurring mainly upon the more dense plate for dissimilar material combinations [14].

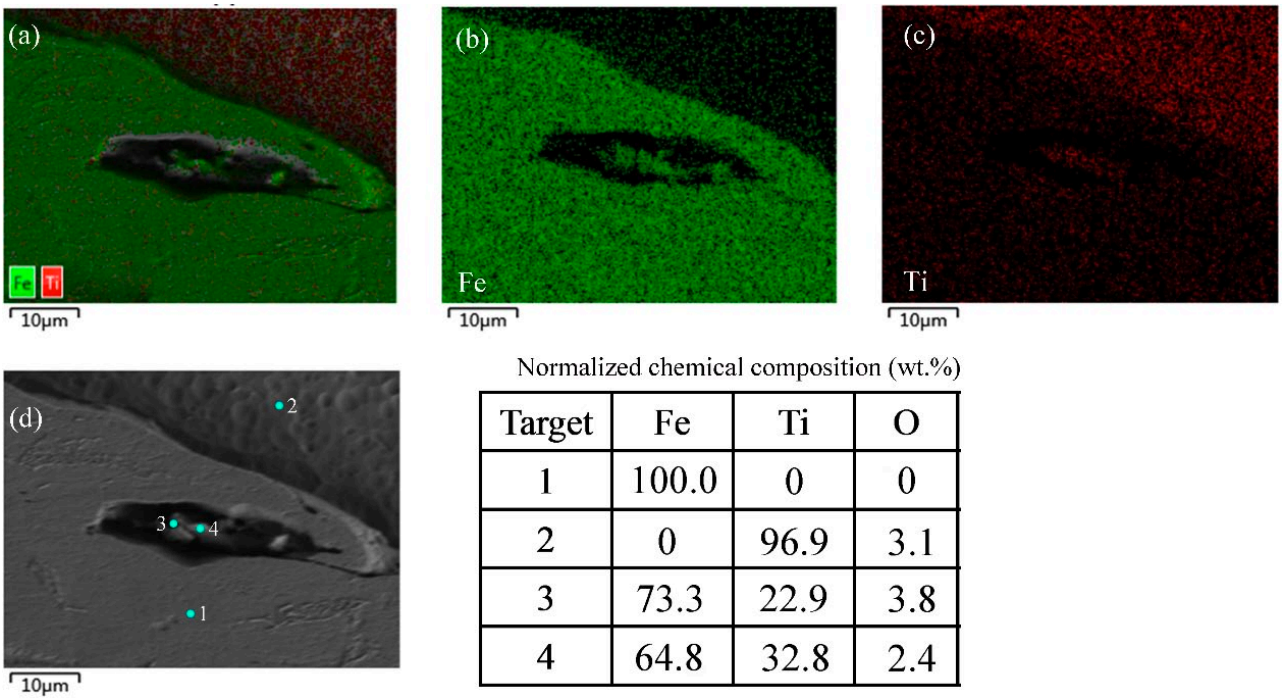

Normalized chemical composition (wt.%)

Target	Fe	Ti	O
1	100.0	0	0
2	0	96.9	3.1
3	73.3	22.9	3.8
4	64.8	32.8	2.4

Fig. 7. EDS mapping and spot scanning near a vortex from weld performed with 60 mm in covering thickness

3.2. Tensile tests

Fig. 8 shows typical stress-strain curves obtained from tensile tests, and the values of tensile strength and elongation are listed in TABLE 6. It can be seen from Fig. 8 that the tensile strength and the elongation decreased with increasing thickness of covering. The decrease in elongation can be related to work hardening. During the welding process, the high-speed oblique collision produces a severe plastic deformation in the welding zones, which can significantly reduce ductility of metals. As shown in TABLE 5, the impact velocity of flyer plate dramatically increases with the increase of covering thickness. Thus, the degree of work hardening increased gradually with increasing covering thickness. The decrease in tensile strength can be attributed to formation of cooling cavities and brittle intermetallics. As shown in Fig. 5, the melting zone increases gradually with the increase of the covering thickness, due to more kinetic energy being converted into heat energy. Typical defects such as voids, crack, and brittle intermetallics are easy to form in these melting zones, which can deteriorate the properties of bonding interface.

Fig. 9 shows the fractographies of samples after tensile tests. As shown in Fig. 9a and b, numerous ductile dimples with large size were observed on both the TA2 side and the Q235

TABLE 6

Tensile test results

Samples	Tensile strength (MPa)	Elongation (%)
T = 0 mm	514±9	12.6±3.2
T = 15 mm	503±6	11.8±2.1
T = 30 mm	498±8	11.4±2.4
T = 60 mm	485±9	10.7±2.8
T = 100 mm	477±11	8.2±3.3

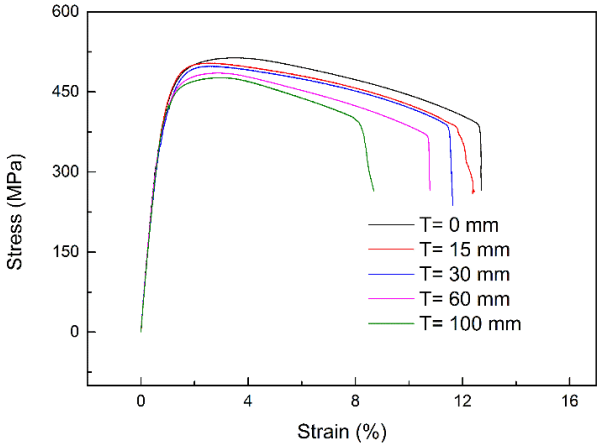

Fig. 8. Typical stress-strain curves obtained by tensile tests

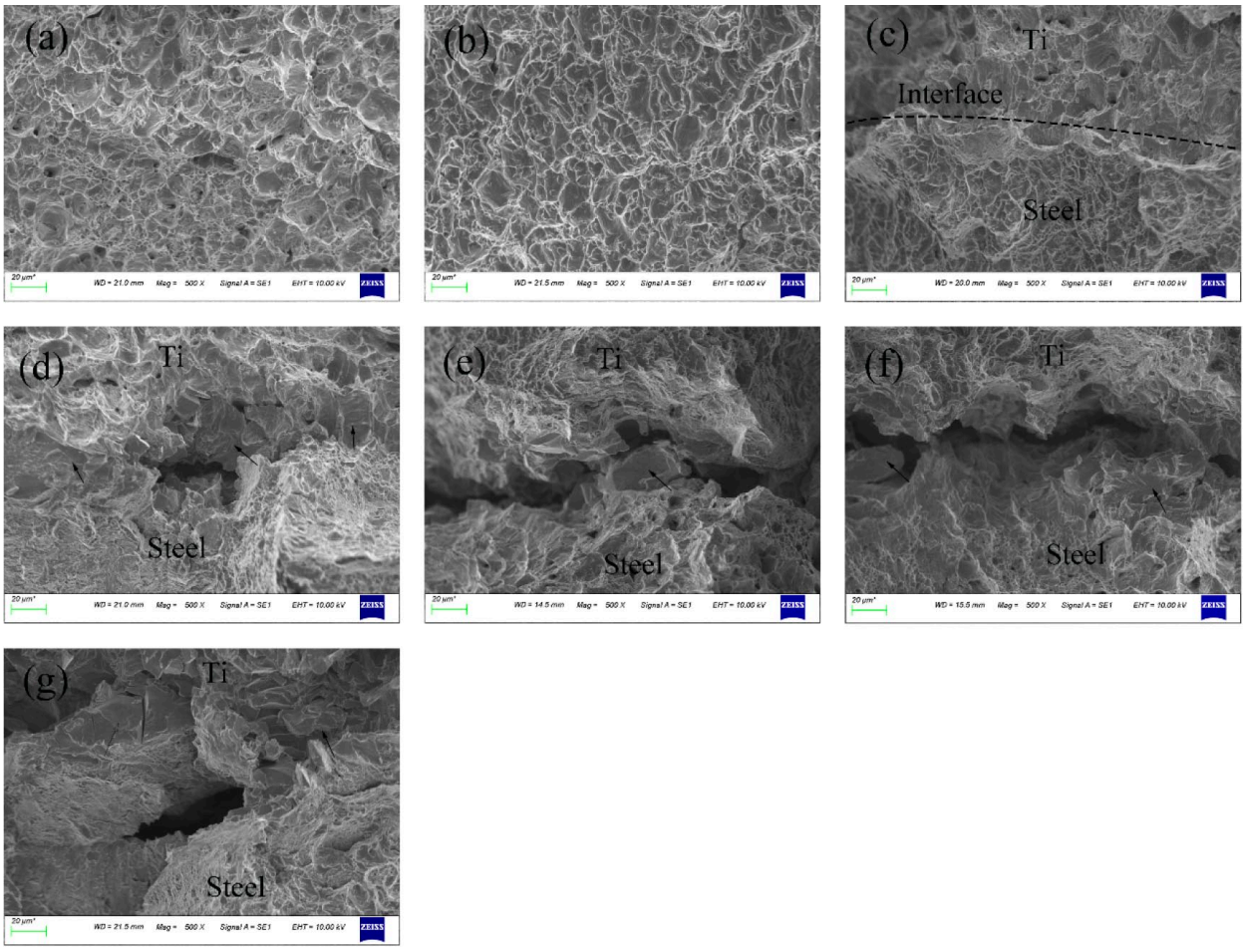

Fig. 9. Fractography after tensile tests, (a) TA2 side away from the interface, (b) Q235 side away from the interface, (c-g) TA2/Q235 bonding interface for different covering thicknesses: (c) T = 0 mm, (d) T = 15 mm, (e) T = 30 mm, (f) T = 60 mm, (g) T = 100 mm

side away from the interface, which were typical characteristics of ductile fracture. Fig. 9c-g are fracture morphologies of the bonding interface, which show a varied fracture characteristic for different covering thicknesses. For no covering, it can be seen from Fig. 9c that no separation happened between the bonding interfaces, and the interface exhibited unambiguous characteristics of ductile fracture with dimples. This is also the reason for obtaining higher tensile strength and elongation in this condition, as shown in Fig. 8. However, Fig. 9d-g show that the bonding interfaces were partly delaminated and cleavage fracture with river pattern (marked by black arrow in Fig. 9d-g) could be found in local zones, due to the effect of work hardening. In this situation, owing to the low ductility of this region containing some brittle intermetallic phases and severely deformed grains, some cracks were initiated at the interface and propagated along the tensile direction [39]. Thus, the tensile strength and the elongation decreased with increasing thickness of covering, as indicated in Fig. 8. It can also be seen from Fig. 9 that the fractures of the bonding interface changed from ductile to cleavage fracture with the increasing covering thickness, due to the increase of impact velocity.

3.3. Tensile shear tests

Shear strength is an important index for assessing transition joints and a key parameter in the application. The results of tensile-shear tests are shown in TABLE 7. As shown in Fig. 10, the fracture took place in the TA2 side, and no separation was observed in the bonding interface in all cases. This result showed that the strength of interface was higher than that of the titanium plate, which was consistent with the previous studies about the shear tests of the titanium/ steel interface produced by explosive welding [40]. This is due to formation of good metallurgical bonding with wavy, as shown in Fig. 5, which is characterized by high bonding strength. It can be seen from TABLE 7 that the tensile-shear strength values varied in the range of 250 to 290 MPa for different covering thicknesses. In some previous studies [40], it was found that the tensile-shear strength values increased with increasing explosive loading, due to the increase of titanium strength. However, this trend was not observed in this work. Although the impact velocity increased as the covering thickness increased, the tensile-shear strength values varied randomly with the change of covering thickness. This could be due to formation of the defects near the bonding interface, which affected the tensile strength of the titanium in a negative manner.

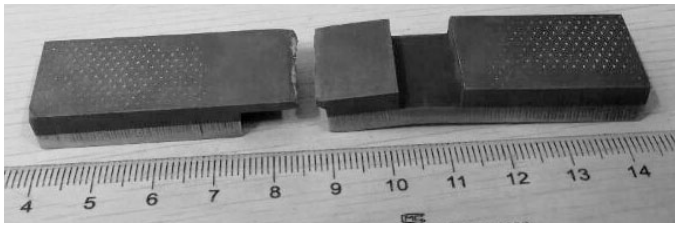

Fig. 10. Typical image of sample after tensile-shear test

TABLE 7

Tensile shear test results

Samples	Shear strength (MPa)
T = 0 mm	≥280±12
T = 15 mm	≥264±13
T = 30 mm	≥253±9
T = 60 mm	≥269±12
T = 100 mm	≥287±14

3.4. Microhardness tests

Fig. 11 is the test results of the microhardness near the interface, where the microhardness line scans were performed across the interface away from the larger volumes of molten zone. As shown in Fig. 11, the micro-hardness generally decreased with increasing distance from the welding interface, due to the work hardening caused by severe plastic deformation in the welding zones. Similar results have been reported by many researchers [15,20,21,40]. Fig. 11 also shows that the microhardness values near the interface increased with increasing thickness of a covering. During the explosion process, the covering can not only reduce the negative effect of the air rarefaction wave on the detonation, but also restrain the upward motion of the detonation products. Thus, the energy of the explosive transferring to the flyer plate increased with increasing thickness of a covering, which resulted in a higher impact energy at the bonding interface. It is clear that the impact energy is proportional to degree of work hardening, so higher microhardness values are observed with increasing thickness of a covering. In addition, it should be noted that the temperatures in near the interface layers also increases with increasing impact energy, due to the existence of shear stresses at the interface layers. In this condition, larger volumes of molten zone are formed and the surrounding parent materials will undergo intense recovery and recrystallization, which eventually leads to a material softening and a decrease in hardness in the very thin layers directly adhering to the interface, as observed in Cu/Al welding system [37]. However, this phenomenon was not observed in this work, where the microhardness value increases monotonically as the distance from the interface decreases. This could be due to the fact that microhardness test lines are away from the larger volumes of molten zone and the thermal conductivity of Ti and Fe is low, which leads to a very thin softening layer that can not be identified using relatively macro hardness indentation. Fig. 12 shows the micro-hardness values near a vortex. It can be seen from Fig. 12 that the microhardness in the vortex was 1078.4 HV, which was far higher than the 312.7 HV hardness of TA2 and 216.1 HV hardness of Q235 near the interface. It means that intermetallic compounds characterized by high hardness, such as TiFe and Ti_2Fe, were formed in the vortex. This result was consistent with the previous studies [21]. It should be noted that the increases of microhardness caused by work hardening and existence intermetallic compounds are quite different aspects, where the work hardening is due to severe deformed grains,

while the intermetallic compounds are the new phases with a hard nature which are formed under the condition of local high temperature and intense mixing of participant metals. Generally, the micro-hardness inside the melting zones is several times higher than that observed in strain-hardened layers of the parent metal.

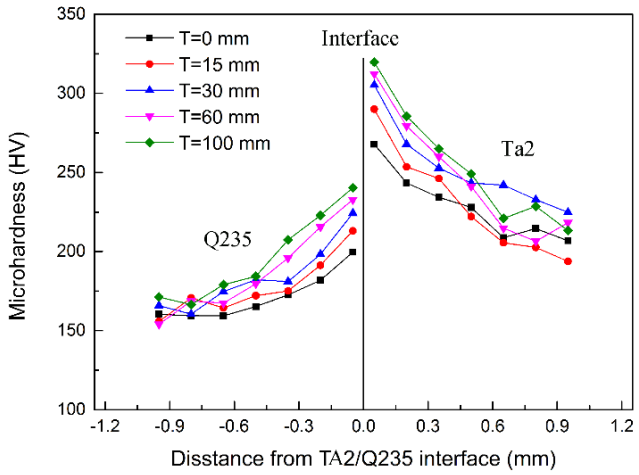

Fig. 11. Microhardness profiles near the bonding interfaces

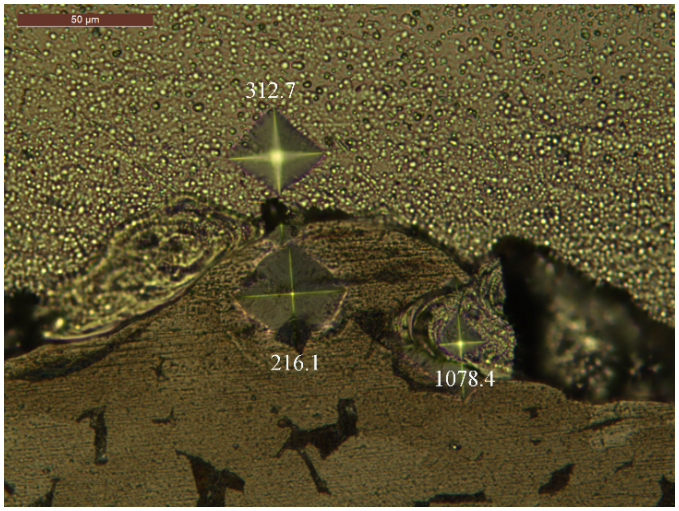

Fig. 12. Microhardness out and inside of the vortex

5. Conclusions

In this work, TA2 titanium and Q235 steel were explosively welded by employing colloid water as a covering for explosives, and the effect of covering thickness on microstructures and mechanical properties of bonding interface was systematically investigated. The following conclusions can be drawn from this study:

(1) All the welds displayed wavy interfaces, and the wavelength and amplitude increased with the increase of covering thickness.

(2) Vortices characterized by localized melting zone surrounded by strongly deformed bulk materials were formed for the welds performed with a covering, and the EDS results indicated that the vortice mainly contained the base plate material.

(3) The tensile strength and the elongation decreased with increasing thickness of covering, due to formation of defects and work hardening at the bonding interface.

(4) The fractographies of the tensile samples changed from ductile to cleavage fracture with the increasing covering thickness.

(5) In the tensile-shearing tests, fracture took place in the TA2 side, and no separation was observed in the bonding interface in all cases, which showed high bonding quality for all welds.

(6) The micro-hardness generally decreased with increasing distance from the welding interface, and the microhardness values near the interface increased with increasing thickness of a covering. In addition, the micro-hardness of the vortex was far higher than that of TA2 and Q235 near the interface, due to formation of hard intermetallic compounds.

Acknowledgements

The reported research is supported by Natural Science Foundation of the Anhui Higher Education Institution (No. KJ2021A0461), Independent subject of State Key Laboratory of Mining Response and Disaster Prevention and Control in Deep Coal Mines (No.SKLMRDPC20ZZ07), Natural Science Foundation of Anhui Province (No. 2108085QA40), University-level key projects of Anhui University of science and technology (No. xjzd2020-03).

REFERENCE

[1] K. Ishida, Y. Gao, K. Nagatsuka, M. Takahashi, K. Nakata, J. Alloy. Compd. **630**, 172-177 (2015).

[2] T.T. Zhang, W.X. Wang, J. Zhou, X.Q. Cao, W. Zhang, JOM-USL. **70**, 504-509 (2017).

[3] D.H. Yang, Z.A. Luo, G.M. Xie, R.D.K. Misra, Mater. Sci. Tech-Lond. **34**, 1700-1709 (2018).

[4] J. Ning, L.J. Zhang, G.C. Jiang, M.X. Xie, X.Q. Yin, J.X. Zhang, J. Alloy. Compd. **701**, 587-602 (2017).

[5] G. Pardal, S. Ganguly, S. Williams, J. Vaja, Int. J. Adv. Manuf. Tech. **86**, 1139-1150 (2016).

[6] T.N. Prasanthi, C. Sudha, S. Saroja, N.N. Kumar, G.D. JanakiRam, Mater. Des. **88**, 58-68 (2015).

[7] Y. Gao, K. Nakata, K. Nagatsuka, F.C. Liu, J. Liao, Mater. Des. **65**, 17-23 (2015).

[8] A.N. Cherepanov, V.I. Mali, I.N. Maliutina, Int. J. Adv. Manuf. Tech. **90**, 3037-3043 (2017).

[9] Y. Zhang, D. Sun, X. Gu, H. Li, Mater. Lett. **185**, 152-155 (2016).

[10] T. Pasang, S Pramana, M. Kracum, W. Misiolek, M. Aziziderouei, M. Mizutani, O. Kamiya, Metals. **8**, 863 (2018).

[11] Q. Chu, M. Zhang, J. Li, C. Yan, Z. Qin, J. Mater. Process. Tech. **240**, 293-304 (2017).

[12] C. Yu, Z.C. Qi, H. Yu, C. Xu, H. Xiao, J. Mater. Eng. Perform. **27**, 1664-1672 (2018).

[13] J. Song, A. Kostka, M. Veehmayer, D. Raabea. Mater. Sci. Eng. A. 5**28**, 2641-2647 (2011).
[14] P. Manikandan, K. Hokamoto, M. Fujita, K. Raghukandan, R. Tomoshige, J. Mater. Process. Tech. **195**, 232-240 (2008).
[15] M. Gloc, M. Wachowski, T. Plocinski, K. Kurzydlowski, J. Alloy. Compd. **671**, 446-451 (2016).
[16] S.A.A.A. Mousavi, P.F. Sartangi, Mater. Sci. Eng. A. **494** 329-336 (2008).
[17] M. Wachowski, M. Gloc, T. Ślęzak, T. Płociński, K.J. Kurzydłowski, J. Mater. Eng. Perform. **26**, 945-954 (2017).
[18] T.N. Prasanthi, C. Sudha, S. Saroja, Mater. Des. **93**, 180-193 (2016).
[19] S.A.A. Akbari Mousavi, P.F. Sartangi, Mater. Des. **30**, 459-468 (2009).
[20] Q. Zhou, R. Liu, C. Ran, K. Fan, J. Xie, P. Chen. Mater Sci. Eng. A **830**, 142260 (2022).
[21] Q. Chu, M. Zhang, J. Li, C. Yan. Mater Sci. Eng. A. **689**, 323-331 (2017).
[22] J. Ning, L.J. Zhang, M.X. Xie, H.X. Yang, X.Q. Yin, J. Alloy. Compd. **698**, 835-851 (2017).
[23] F. Fındık, Mater. Des. **32**, 1081-1093 (2011).
[24] T.Z. Blazynski, Elsevier, New York (1983).
[25] Q. Zhou, J. Feng, P. Chen, Materials **10**, 984 (2017).
[26] V.I. Lysak, S.V. Kuzmin. J. Mater. Process. Tech. **222**, 356-364 (2015).
[27] C. Borchers, M. Lenz, M. Deutges, H. Klein, F. Gärtner, M. Hammerschmidt, H. Kreye, Mater. Des. **89**, 369-376 (2016).
[28] R. Mendes, J.B. Ribeiro, A. Loureiro, Mater. Des. **51**, 182-192 (2013).
[29] A. Durgutlu, H. Okuyucu, B. Gulenc, Mater. Des. **29**, 1480-1484 (2008).
[30] M. Yang, H. Ma, Z. Shen, Int. J. Adv. Manuf. Technol. **99**, 3123-3132 (2018).
[31] GB/T6396-2008, China National Standardization Management Committee, May 13, 2008.
[32] H.B. Xia, S.G. Wang, H.F. Ben, Mater. Des. **56**, 1014-1019 (2014).
[33] Bina, M. Hosein, F. Dehghani, M. Salimi, Mater. Des. **45**, 504-509 (2013).
[34] S.A.A.A. Mousavi, S.T.S. Al-Hassani, Mater. Des. **29**, 1-19 (2008).
[35] A.A. Deribas, V.M. Kudinov, F.I. Matveenkov, Combust. Explo. Shock Waves **3**, 344-348 (1967).
[36] A.A. Mousavi, S.T.S. Al-Hassani, J. Mech. Phys. Solids. **53**, 2501-2528 (2005).
[37] H. Paul, L. Lityńska-Dobrzyńska, M. Prażmowski, Metall. Mater. Trans. A. **44**, 3836-3851 (2013).
[38] P. Manikandan, K. Hokamoto, A.A. Deribas, K. Raghukandan, R. Tomoshige, Mater. Trans. **47**, 2049-2055 (2006).
[39] M.M. Hoseini-Athar, B. Tolaminejad, Met. Mater. Int. **22**, 670-680 (2016).
[40] N. Kahraman, B. Gülenç, F. Findik, J. Mater. Process. Tech. **169**, 127-133 (2005).
[41] H. Paul, M.M. Miszczyk, R. Chulist, M. Prażmowski, J. Morgiel, A. Gałka, F. Brisset. Mater. Des. **153**, 177-189 (2018).
[42] H. Paul, J. Morgiel, M. Faryna, M. Prażmowski, M.M. Miszczyk, Int. J. Mater. Res. **106**, 782–792 (2015).
[43] I.A. Bataev, S. Tanaka, Q. Zhou, D.V. Lazurenko, A.J. Junior, A.A. Bataev, P. Chen, Mater. Des. **169**, 107649 (2019).
[44] I.A. Bataev, D.V Lazurenko, S. Tanaka, K. Hokamoto, A.A. Bataev, Y. Guo, A.M. Jorge Jr, Acta Materialia **135**, 277-289 (2017).